Supplementary material

CO_2 capture from ships: An in-depth multi-criteria screening of CO_2 capture technologies

[1]Donghoi Kim[*], [1]Sai Gokul Subraveti, [1]Rahul Anantharaman, [2]Sadi Tavakoli, [1]Simon Roussanaly

[1]Department of Gas Technology, SINTEF Energy Research, Norway

[2]Department of Energy and Transport, SINTEF Ocean, Norway

[*]Corresponding author's Email: Donghoi.Kim@sintef.no

S.1 Ship energy balance and specifications

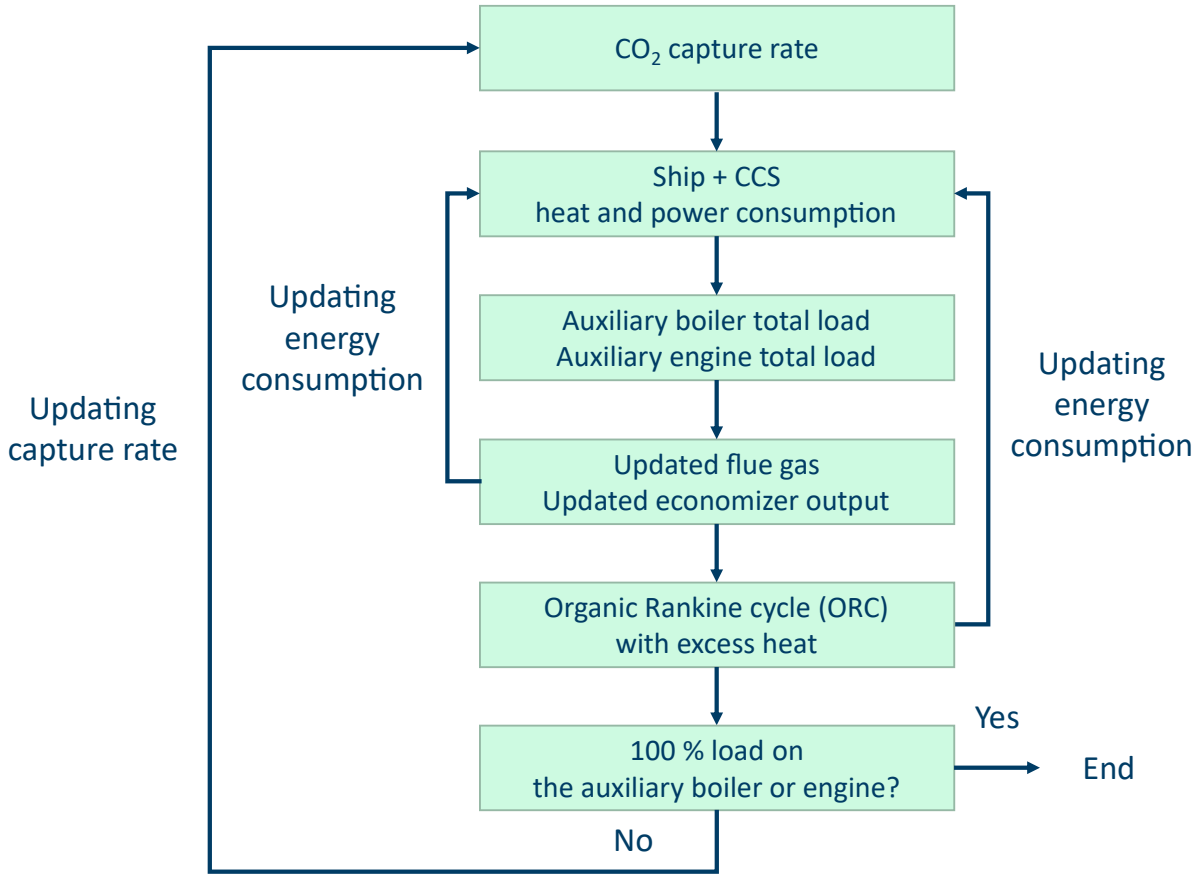

Figure S-1. Energy balance tool for ship power systems with OCCS.

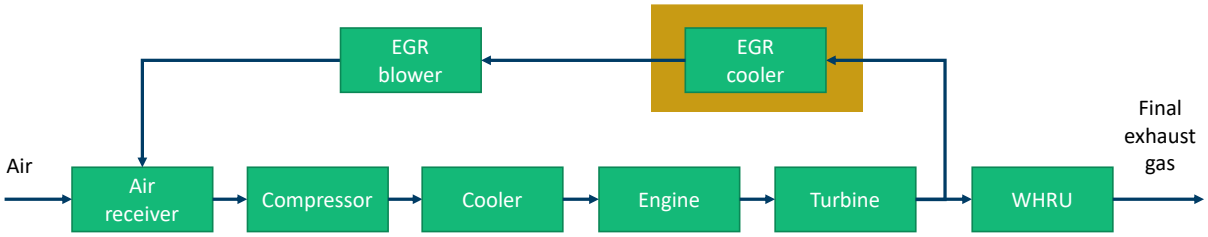

Figure S-2. The EGR configuration assumed for the newbuilding case (Gold color: potential heat recovery point).

Table S-1. Key specifications of the main propulsion engine without CCS.

Item	Unit	Retrofit Diesel engine	Newbuilding Diesel engine with EGR
Number of engines	-	1	1
Engine nominal capacity	MW	9.6	9.6
Actual engine load	%	85	85
Actual engine duty	MW	8.16	8.16
Fuel type	-	HFO	HFO
EGR rate	%	-	41
Specific fuel consumption	g/kWh	169	172
Flue gas temperature	°C	260	260
Flue gas pressure	kPa	105.9	105.9
Flue gas mass flow rate	kg/h	48482	36073
Flue gas c_p	kJ/kg-C	1.084	1.077
Flue gas CO_2 mass flow rate	kg/h	4391	4458
Flue gas CO_2 concentration	mol%	5.97	8.16
Recoverable waste heat	MW_{th}	1.24	0.91

Table S-2. The specifications of the auxiliary engines at the baseload condition without CCS.

Item	Unit	Type 1	Type 2
Number of engines	-	2	1
Engine nominal capacity	MW	1.35	0.81
Generator efficiency	%	95	95
Generator output at nominal capacity	$MW_{el.}$	1.28	0.77
Actual engine load	%	15.04	15.04
Actual engine duty	$MW_{el.}$	0.19	0.12
Fuel type	-	HFO	HFO
Specific fuel consumption	g/kWh	180	180
Flue gas temperature	°C	260	260
Flue gas pressure	kpa	106.33	106.33
Flue gas mass flow rate	kg/h	1280	769.9
Flue gas CO_2 mass flow rate	kg/h	115.9	69.8
Flue gas CO_2 concentration	mol%	5.97	5.97

Table S-3. The specifications of the auxiliary boiler at the baseload condition without CCS.

Item	Unit	Value
Number of saturate steam boilers	-	1
Steam pressure	bara	7
Steam temperature	°C	165
Steam generation capacity	kg/h	11000
Boiler nominal capacity	MW_{th}	6.29
Boiler actual load	%	13.52
Boiler actual duty	MW_{th}	0.85
Actual steam mass flow rate	kg/h	1487
Fuel type	-	HFO
Fuel lower heating value	MJ/kg	41.80
Boiler thermal efficiency	%	85
Flue gas temperature	°C	225
Flue gas pressure	bara	1.04
Flue gas mass flow rate	kg/h	1595
Flue gas CO_2 mass flow rate	kg/h	276
Flue gas CO_2 concentration	mol%	11.41

Table S-4. The specifications of the WHRU at the baseload condition without CCS.

Item	Unit	Retrofit HFO	Newbuilding HFO-EGR
Number of WHRU	-	1	1
Steam pressure	bara	7	7
Steam temperature	°C	165	165
Steam generation capacity	kg/h	var	Var
WHRU actual load	MW_{th}	1.35	1.04
Produced steam m	kg/h	2369	1817
Flue gas exit temperature	°C	175	175
Flue gas exit pressure	kpa	104.4	104.4
Flue gas mass flow rate	kg/h	53407	41587

S.2 CO_2 Capture processes

S.2.1 Absorption

Figure S-3 presents the process flow diagram of a typical chemical absorption process employing aqueous monoethanolamine (MEA) as a solvent.

As illustrated in Figure S-3, this work applies a standard configuration to the absorption process using MEA. Although alternative process configurations, such as absorber intercooling [2,3] and rich solvent bypass [4], can potentially improve capture efficiency, but their increased process complexity will make them less attractive for marine applications. Thus, they are not considered in the retrofit or newbuilding case.

In this process, the exhaust gas is first cleaned via a direct contact cooler (DCC) to remove SOx by NaOH before being fed to the capture system. The DCC outlet gas is then sent to an absorber column to capture CO_2 by MEA. The CO_2-rich solvent from the bottom of the absorber is heated by the rich/lean solvent heat exchanger and sent to a stripper column to separate CO_2 through external heat provided by a reboiler. The high-purity CO_2 stream is then fed to a condenser to collect the solvent left in the gas. The CO_2-lean solvent from the reboiler is then returned to the absorber column after delivering heat to the rich solvent in the rich/lean solvent heat exchanger.

Since this absorption process primarily requires heat, it is suitable for ships with a large boiler and a waste heat recovery unit for the exhaust gas, such as the target ship of this study. The boiler and WHRU are also connected to a steam generation system, which can easily supply the reboiler duty. In addition, the high TRL of the absorption systems makes deployment less challenging than that of other capture technologies. Therefore, this study selects the chemical absorption CO_2 capture process as a baseline for comparison with alternative technology solutions.

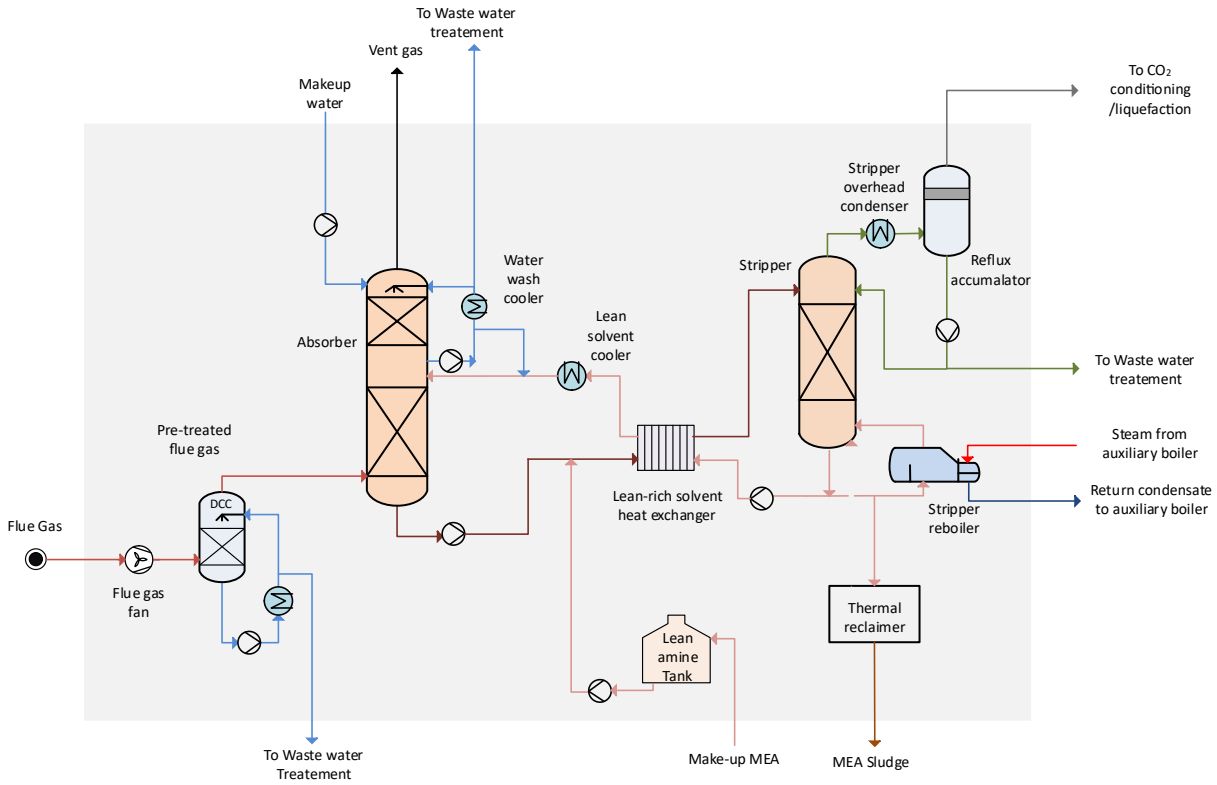

Figure S-3. Process flow diagram of chemical absorption CO_2 capture process using MEA.

The optimal configuration is also influenced by part-load performance, given the large fluctuations in ship speed and engine load during a voyage [5]. However, this aspect is beyond the scope of the present study. In addition, process intensification, such as solvent selection and lean loading optimization, is not included in this initial screening stage.

The absorption process is modeled and simulated using Aspen HYSYS, validated in previous studies [5–7]. During the simulation, the maximum height is constrained due to the space limitations on the target ship. The limited height of the absorber and desorber columns will influence the energy efficiency of the capture process. It is, however, worth noting that the capture rate is also limited by the available heat and power on the ship for the retrofit case, which reduces the energy demand of the process. The design specifications and simulation results for the absorption system can be found in Sections S.3 and S.4.

S.2.2 Membrane-liquefaction hybrid

Membrane-based separation is an emerging technology for post-combustion CO_2 capture with various advantages, including no steam requirement, compactness, relatively easy retrofitting, and reduced environmental impacts compared to solvent-based systems [8]. However, several limitations make membranes hard to deploy, such as membrane selectivity and permeability, the need for multi-stage processes, and significant feed gas compression to attain high CO_2 purity and recovery targets. Stand-alone membrane processes are also known for being more energy-intensive than amine-based solvent technology [9]. Besides, membrane-based CO_2 capture systems are purely electricity-driven, and the capacity and performance of membrane-based capture depend on the amount of electricity available on a ship. Otherwise, a larger amount of fuel will be needed to generate additional electricity for the CCS unit, increasing CO_2 emissions and, thus, the size of the capture facility onboard.

To overcome these limitations, membrane-assisted CO_2 liquefaction has been explored in the literature [8,10]. As shown in Figure S-4, the membrane/liquefaction hybrid is based on a combination of two different separation technologies, membranes and low-temperature CO_2 liquefaction. Neither of these technologies is suited as a stand-alone system for exhaust gases with low CO_2 concentration due to the significant energy penalty [10]. The main idea is to perform partial separation using each technology within its favorable operation regime [8,10]. First, the membranes are used for bulk separation of CO_2 with moderate product purity. Following this, the low-temperature CO_2 liquefaction is used to concentrate the CO_2 further to obtain a high-purity CO_2 product at storage conditions. This hybrid will reduce the power consumption of the CCS system compared to membrane or liquefaction stand-alone processes while keeping the facility compact.

Figure S-4 presents that the exhaust gas is cleaned and cooled by a DCC before being compressed and sent to a membrane module to separate CO_2. The permeate gas, which carries CO_2, is pumped from the vacuum to ambient pressure. The permeate gas from the vacuum pump heats the high-pressure retentate gas, which is expanded to generate electricity. Afterward, the permeate gas is cooled to condense and remove water. It is worth noting that the membrane part can be in multiple stages if a high capture rate and high-purity CO_2 product are required. The CO_2-upgraded gas from the membrane part is compressed before being dehydrated and pre-cooled. The pre-cooled CO_2-rich stream is partially condensed by a cascade refrigeration cycle (propane and ethane as refrigerants) to remove impurities through the vapor. The vapor (off-gas) from the liquefier is then sent to the pre-cooler to provide a part of the cold duty for the heat exchanger. Afterward, the high-pressure off-gas is heated by the compressor outlet streams and expanded to generate electricity. Since the off-gas contains CO_2, it is returned to the membrane part to maximize the CO_2 recovery of the hybrid concept.

The condensed liquid from the liquefier provides part of the cold duty to the refrigeration cycle. As it delivers the cold duty, the CO_2-rich liquid is slightly heated, allowing impurities to boil off after throttling. The purified CO_2 is then sent to the pre-cooler to provide cold energy. The flash gas, which contains impurities and some CO_2, is returned to the liquefier to enhance the CO_2 capture rate.

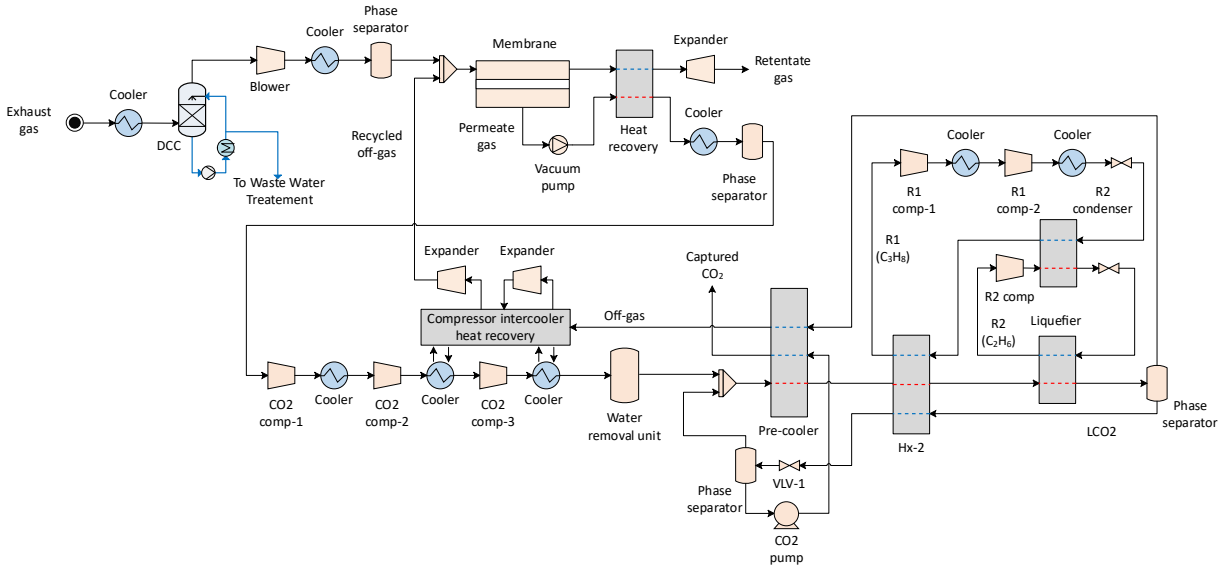

Figure S-4. The process flow diagram of the membrane/liquefaction hybrid CO_2 capture system [8].

To model the hybrid concept, a cross-flow multicomponent membrane model is used during the simulation and linked to Aspen HYSYS to configure other process units [11]. In this work, the Polaris membrane from Membrane Technology and Research, Inc. (MTR) is considered, as shown in Table S-5. Other design specifications and simulation results are presented in Sections S.3 and S.4.

Table S-5. Characteristics of the Polaris membrane [12].

Membrane	CO_2 permeance ($m^3_{(STP)}\ m^{-2}\ h^{-1}\ bar^{-1}$)	Selectivity		
		CO_2/N_2	CO_2/O_2	CO_2/H_2O
Polaris	5.94	50	35	0.3

S.2.3 VSA-liquefaction hybrid

Vacuum swing adsorption (VSA) using solid adsorbents is another promising and emerging post-combustion CO_2 capture technology. This technology has been successfully commercialized for CO_2 capture by Air Products in Port Arthur, Texas, demonstrating a relatively high TRL. In contrast to other technologies, VSA offers additional flexibility in both process design and operation [13]. This characteristic makes it particularly appealing for onboard CO_2 capture from ship exhaust gas, especially considering the constraints of limited heat and power available aboard ships.

Despite this advantage, implementing VSA as a standalone capture technology to achieve high-purity CO_2 for low CO_2 compositions in the exhaust gas poses challenges due to its large footprint, which requires multiple columns and parallel trains to treat the exhaust gas, as well as deep vacuum needs that increase power consumption for maximizing CO_2 purity and capture rate. Instead, VSA can be integrated with CO_2 liquefaction, similar to earlier membrane-liquefaction. In this hybrid process, VSA performs the bulk separation in the first stage to achieve moderate-to-high CO_2 purities, while the subsequent liquefaction process further delivers high-purity CO_2. For instance, Air Liquide deployed a similar hybrid PSA-liquefaction for post-combustion CO_2 capture.

Two VSA cycles are considered for the bulk separation of CO_2 in the first stage. The first cycle, illustrated in Figure S-5, consists of four steps and is employed for the retrofit case study. Due to its simplicity, this cycle has been widely studied [13–15] and benchmarked through lab-scale [16] and pilot-scale [17] demonstrations. Considering the space limitations in a retrofit case, simpler cycles are preferred due to their simplicity and the fewer number of columns needed to implement different steps in the cycle.

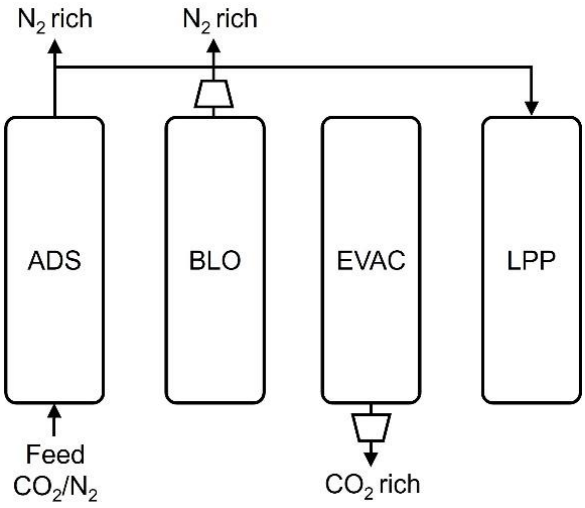

Figure S-5. Four-step vacuum swing adsorption cycle: ADS – feed adsorption, BLO – co-current blowdown, EVAC – counter-current evacuation, and LPP – light product pressurization.

As shown in Figure S-5, the cycle comprises an adsorption step, where exhaust gas feed is introduced into the column at ambient pressure. The separation of CO_2 from the rest of the exhaust gas occurs here through preferential adsorption of CO_2. Following adsorption, the column pressure is reduced to an intermediate vacuum in the co-current blowdown step to remove impurities and enrich the column with CO_2. The CO_2-enriched product is collected in the subsequent counter-current evacuation by further reducing the column pressure to a low vacuum. The column is pressurized back to ambient pressure in light product pressurization using the outlet stream in the adsorption step.

Since high capture rates are targeted in the newbuilding case, a more complex VSA cycle with six steps, shown in Figure S-6, is considered. The six-step VSA cycle retains the four steps from the previous cycle, but includes two additional reflux steps, i.e., light reflux and heavy reflux, to improve the recovery and the purity of CO_2. For more details on both the cycles and their design, the readers are referred to a previous study [18].

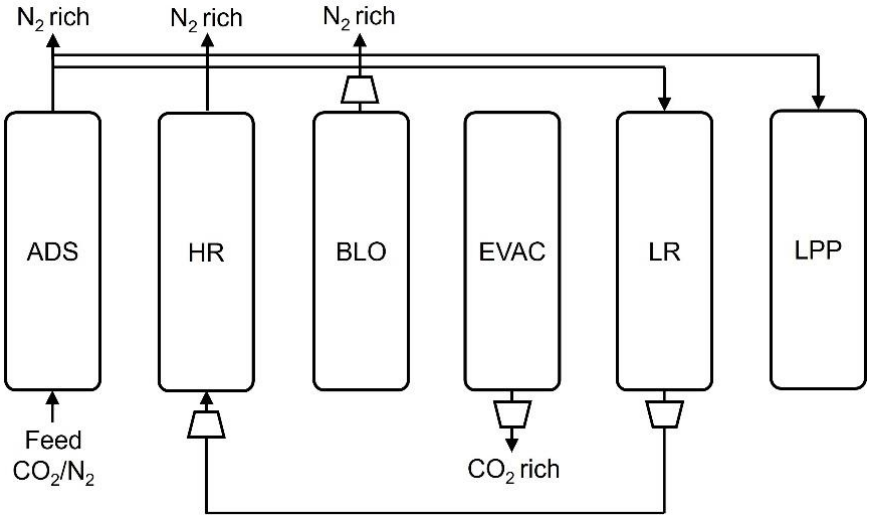

Figure S-6. Six-step vacuum swing adsorption cycle: ADS – feed adsorption, HR – heavy reflux, BLO – co-current blowdown, EVAC – counter-current evacuation, LR – light reflux, and LPP – light product pressurization.

The performance of two VSA cycles is assessed using commercial zeolite 13X as the adsorbent, which serves as the current benchmark for post-combustion CO_2 capture. An integrated process optimization framework is then employed to identify the optimal process performance of the hybrid VSA-liquefaction configuration in each case study. Given the flexibility in tuning several design variables in VSA processes, a multitude of process simulations must be carried out with varying combinations of design variables in the optimizations to identify the optimal solution. The list of design variables in the optimizations and their ranges is provided in Section S.3.

However, adsorption process simulations using rigorous process models are computationally very expensive and time-consuming for use within the integrated process optimizations. Alternatively, data-driven models based on machine learning can be used as a surrogate for rigorous process simulations, which have become increasingly common to rapidly assess the process performance of VSA processes [19–22]. Similarly, surrogate models are developed for the liquefaction process, and these models are incorporated into the integrated optimization routine, which uses non-dominated sorting genetic algorithm II (NSGA-II) as the optimization method.

This study uses artificial neural networks (ANNs) to predict the process performance of two VSA cycles. To generate relevant training data for ANNs, a rigorous one-dimensional process model comprising a set of nonlinear partial differential equations (PDEs) developed in-house [23] was employed. This process simulator follows the modelling procedure outlined in Haghpanah et al. [24] and Subraveti et al. [13]. Briefly, the spatial terms in PDEs were discretized using finite volume methods, and the resulting ordinary differential equations (ODEs) were integrated using the built-in "solve_ivp" solver in Python 3.10, which employs the implicit multi-step variable order method. The model equations, boundary conditions, and competitive dual-site Langmuir isotherm equations used in this study can be retrieved from Subraveti et al. [18]. This approach has been extensively used in adsorption process studies [18,21,22,24] and has been validated experimentally elsewhere [16].

For the four-step VSA cycle, six unique ANN models are trained, each consisting of one input layer with seven neurons, which represent seven process decision variables (CO_2 feed composition, intermediate vacuum in the blowdown step, low vacuum in the evacuation step, adsorption step duration, blowdown and evacuation vacuum pump velocities, and column length), two hidden layers with 20 neurons each, and a single output layer with one neuron, representing a distinct process output (CO_2 purity, CO_2 recovery, VPSA power consumption, blowdown and evacuation step durations, and inlet feed molar flow rate). To train these ANNs, an initial design of experiments using Latin-hypercube sampling is carried out on the process decision variables spanning across a wide range of the design space. Around 900 unique combinations of the input variables were used as samples in the training, which was deemed sufficient to construct high-accuracy ANN models based on previous studies [25–27]. For more details on the ANN training, the readers are referred to an earlier work [27]. An independent dataset was used to test the accuracy of the trained models, and the corresponding parity plots showing the validation of these ANN models are presented in Figure S-. All models achieved a high R2 of >0.96.

Similarly, eight unique ANN models are trained for the six-step VSA cycle. The ANN architecture includes an input layer with nine neurons (each corresponding to the previous seven process decision variables and two additional inputs, i.e., light reflux inlet velocity and the fraction of the adsorption outlet stream that goes as an inlet stream in the light reflux step), two hidden layers with 20 neurons each, and a single output layer with one neuron. The outputs for this cycle include CO_2 purity, CO_2 recovery, VPSA power consumption, blowdown and evacuation step durations, light reflux outlet flow rate, heavy reflux inlet flow rate, and inlet feed molar flow rate. In the training, ~1200 samples with unique combinations of process design variables were used, and the model validation using an independent test dataset can be visualized through parity plots shown in Figure S-. Again, all models achieved high accuracy, as demonstrated by R2>0.95.

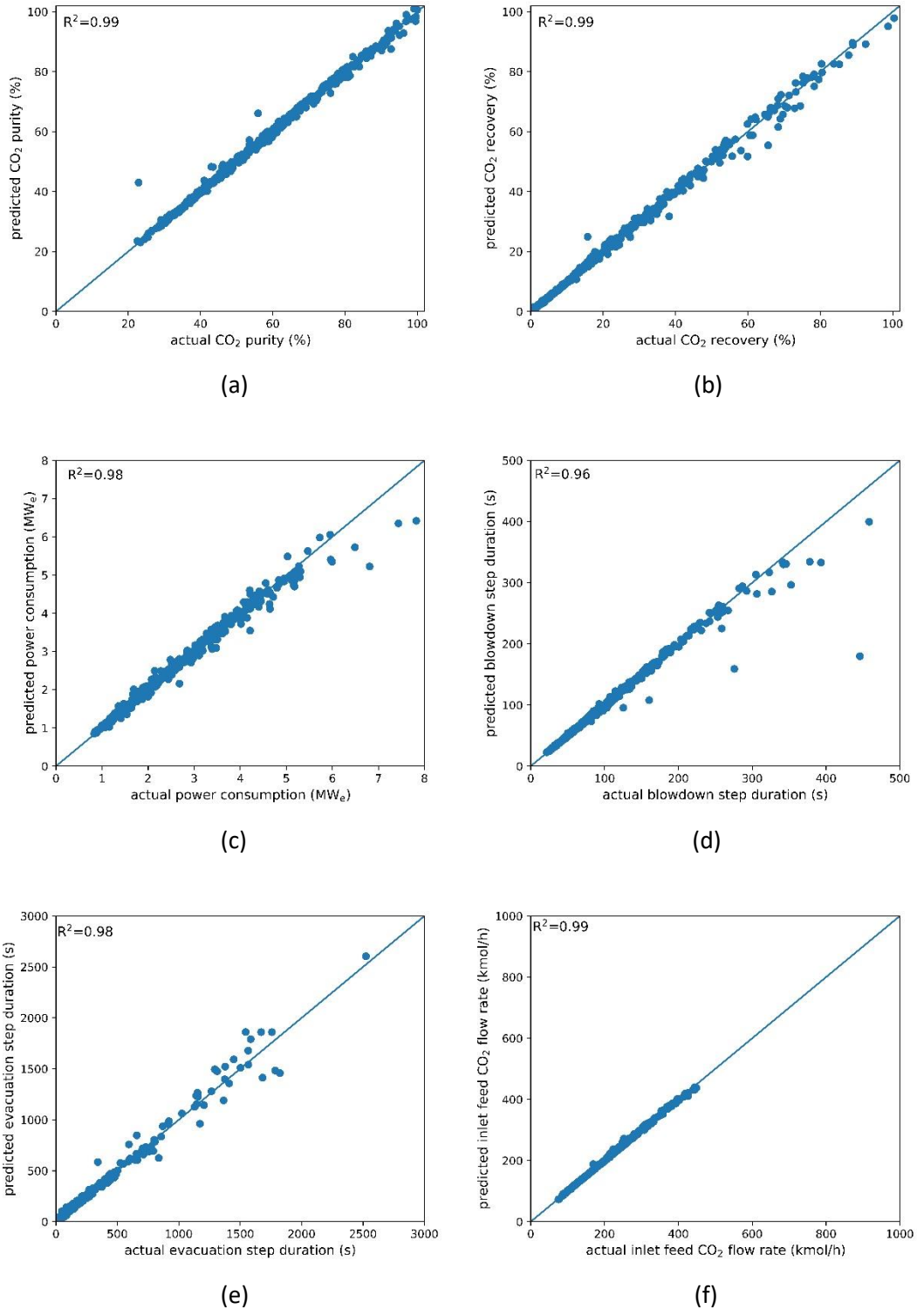

Figure S-7. Parity plot of the rigorous process model (actual) and ANN model (predicted) for an independent test dataset shown for (a) CO_2 purity, (b) CO_2 recovery, (c) VPSA power consumption, (d) blowdown step duration, (e) evacuation step duration, and (f) inlet feed CO_2 molar flow rate.

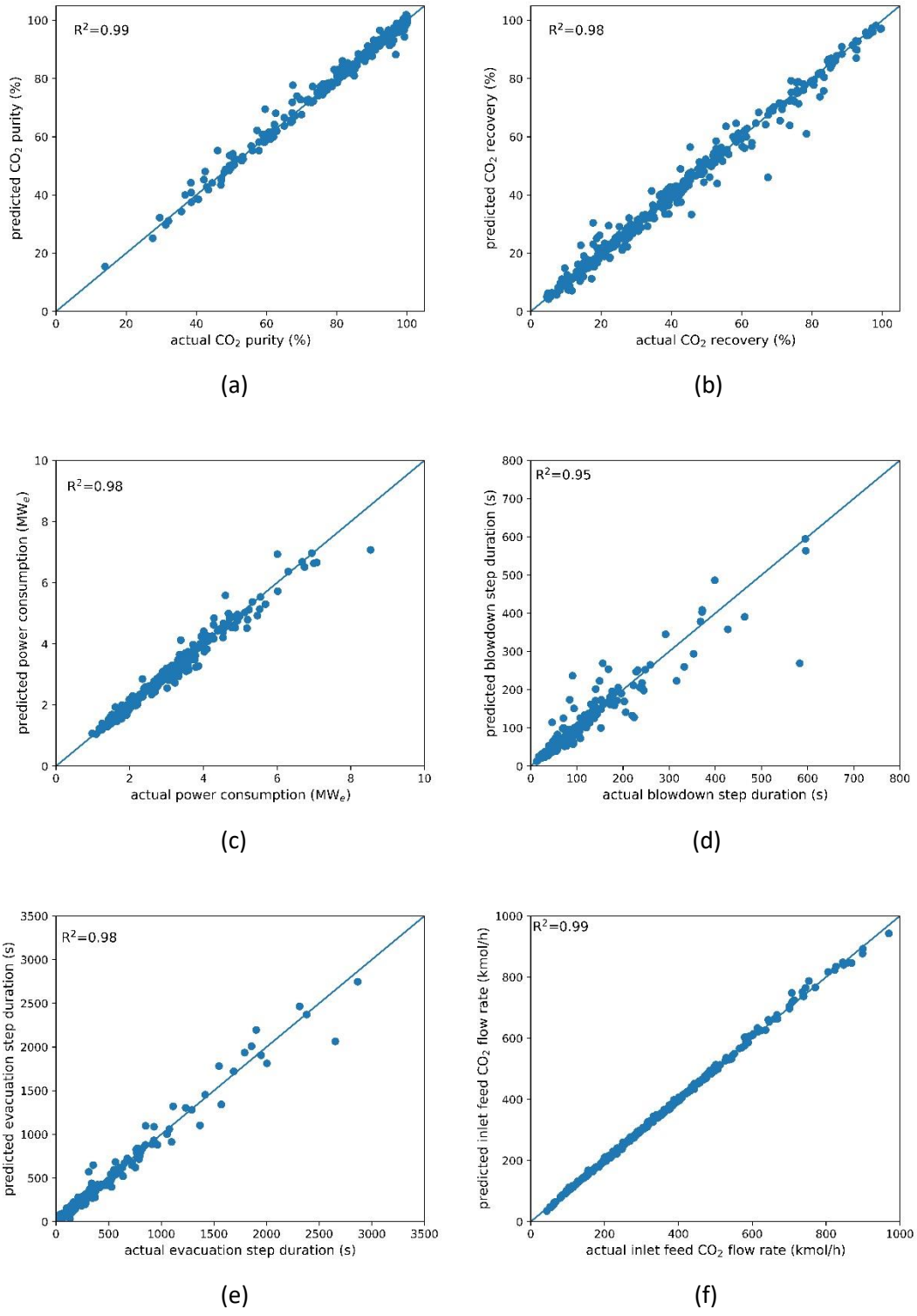

Figure S-9. Parity plot of the rigorous process model (actual) and ANN model (predicted) for an independent test dataset shown for (a) CO_2 purity, (b) CO_2 recovery, (c) VPSA power consumption, (d) blowdown step duration, (e) evacuation step duration, and (f) inlet feed CO_2 molar flow rate.

S.2.4 CaL and CaL-absorption hybrid

Calcium looping (CaL) is a CO_2 capture process based on limestone ($CaCO_3$) involving calcination and carbonation reactions. The calcium carbonate is first sent to a furnace or a fluidized bed reactor (calciner) to produce CO_2 and CaO. The sorbent (CaO) is then recycled to the carbonator reactor, where it reacts with CO_2 in the flue gas to form $CaCO_3$. The CO_2-rich sorbent is then returned to the calciner for CO_2 separation. In standard operations, the carbonator operates at 600 °C while the calciner runs at 900 °C, making onboard deployment challenging [28]. To address this issue, Calix proposes a calcium looping-based application (RECAST) tailored for marine vessels, as illustrated in Figure S- [29].

In this approach, the high-temperature calciner unit is located onshore, where the CO_2-rich sorbent (CaCO3) is calcined to form CaO. The regenerated sorbent (CaO) is then loaded onto a vessel to capture CO_2 from exhaust gases. Once the sorbent is CO_2-rich, it is stored onboard and later unloaded for regeneration in the onshore calciner. Although this concept needs to address several technical challenges, such as onboard solid handling and port infrastructure for limestone, the CaL concept generates heat within the carbonator, reducing the heat demand for ship operation [29]. Hence, as presented in Figure S-8, this screening analysis assumes that only the carbonator is placed onboard while the calciner remains on land (typically near the shipping ports).

From an energy perspective, the CaL process appears ideal for onboard CO_2 capture since it does not require any energy inputs. Instead, the system (carbonator) produces a large amount of high-temperature heat, though managing this heat can be challenging [28]. Thus, the RECAST concept from Calix suggests utilizing the generated heat for running a steam turbine [29]. However, this screening work assumes that the heat from the carbonator is collected through a heat recovery system to generate steam, which simplifies the system for ship applications (see Figure S-8). In addition, the material cost, which will be the main operational burden of this concept, is disregarded due to uncertainty.

This CaL process can be combined with the reference absorption system to share the capture duty, thereby minimizing the required lime storage volume. As presented in Figure S-9, the capacity of the CaL system is adjusted to ensure that the heat from the carbonator is sufficient to cover the reboiler duty of the absorption system and the heat baseload for ship operation. Therefore, the heat from the carbonator can satisfy the total onboard heat demand, minimizing the use of the auxiliary boiler and fuel consumption. However, due to the complex process structure and yet noticeable solid inventory expected, this CaL-absorption hybrid concept is only applied to the newbuilding case in this work.

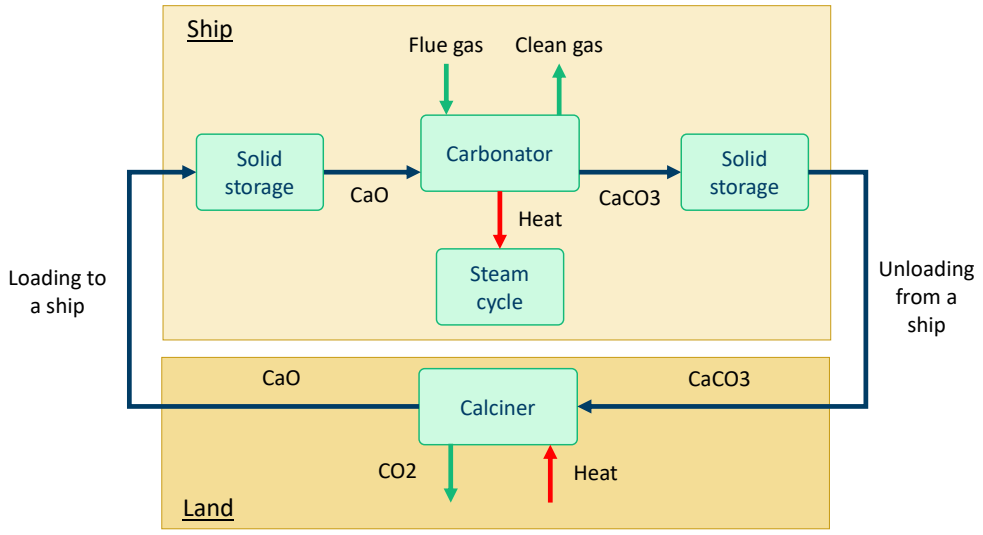

Figure S-10. Process flow diagram of the RECAST concept [29].

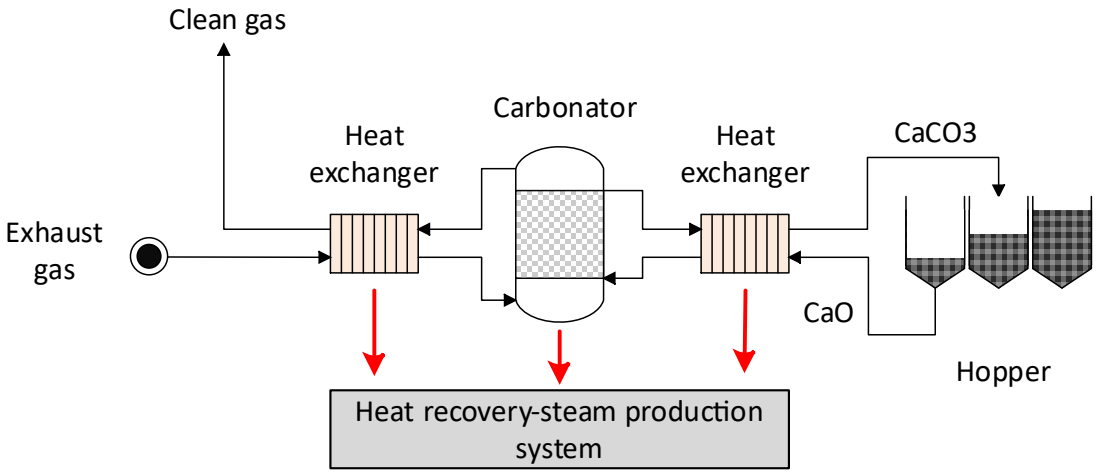

Figure S-8. The process flow diagram of the CaL-based CO_2 capture system.

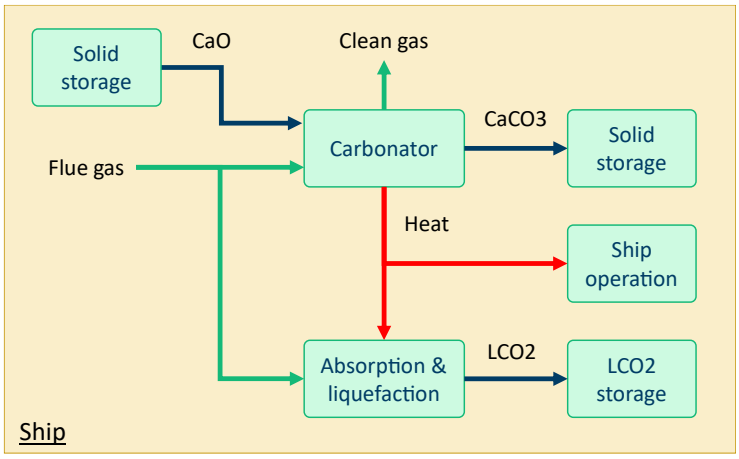

Figure S-9. Process flow diagram of the CaL-absorption hybrid system.

To evaluate the primary performance of the CaL-based technologies, appropriate calculations on heat and space requirements are performed using our in-house simulator. It is worth noting that in the CaL concepts, the exhaust gas is directly supplied to the carbonator system, rather than an economizer, as presented in Figure S-8. The total solid storage capacity is designed to be 25% larger than the total return flow for the 20-day journey, assuming an empty CaO hopper is used for CaCO3 storage, with one of the five hoppers reserved for seamless material transfer.

It is worth noting that the CaL concepts are assumed to utilize a typical cycled sorbent, which exhibits degraded performance in the conversion rate with CO_2 [30]. However, replacing a portion of the cycled sorbent with fresh material increases the conversion rate with CO_2, thereby reducing the required amount of sorbent for CO_2 capture and its onboard storage space. The relationship between the actual conversion rate and the storage requirement is illustrated from Figure S-10 to Figure S-13. A high conversion rate, such as 95 %, corresponds to completely fresh sorbent, whereas typical cycled material has a conversion rate of around 40 %. The figures also indicate that the conversion rate (or the fraction of fresh sorbent) has a minor impact on the carbonator size and waste heat recovered once the conversion rate exceeds the typical cycled sorbent level (around 40 %). Thus, this work considers a typical cycled sorbent and fresh solvent to identify the range of solid storage requirements while assuming unchanged size and waste heat of the carbonator. Other design conditions and process results for the CaL systems are presented in Sections S.3 and S.4.

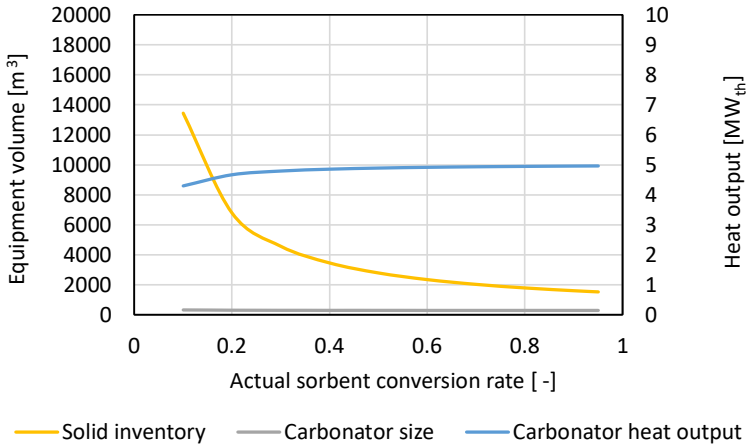

Figure S-10. The impact of sorbent conversion rate in the CaL capture system for the retrofit case.

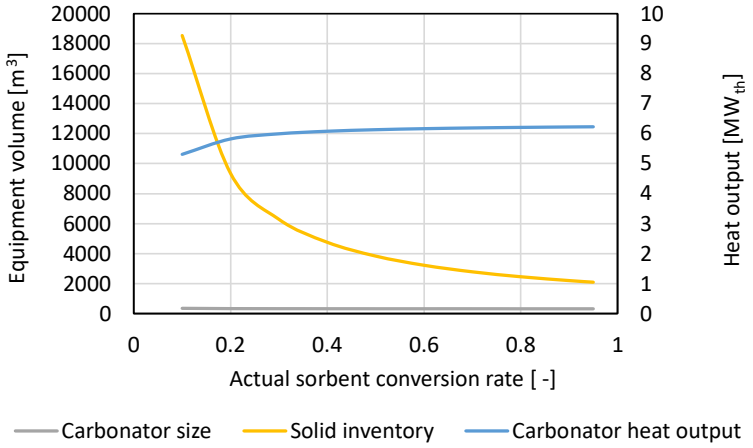

Figure S-11. The impact of sorbent conversion rate in the CaL capture system for the newbuilding case with a 90 % CO_2 capture rate equivalent.

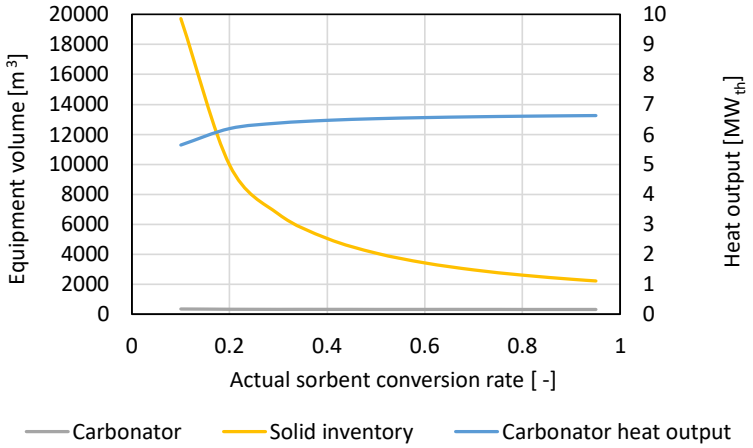

Figure S-12. The impact of sorbent conversion rate in the CaL capture system for the newbuilding case with a 95 % CO_2 capture rate equivalent.

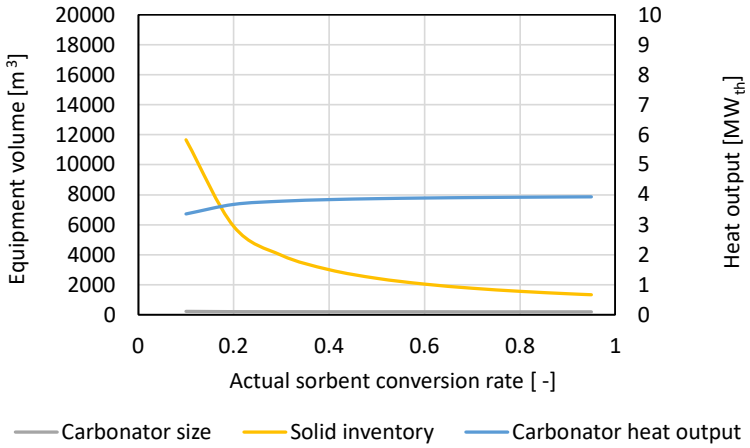

Figure S-13. The impact of sorbent conversion rate in the CaL-MEA hybrid capture system for the newbuilding case.

S.2.5 Cryogenic supersonic separation

The supersonic flow-driven CO_2 deposition is distinctively an alternative approach that was developed by Orbital ATK and ACENT Laboratories [31]. Although the supersonic separation technology was initially introduced to remove water vapor from natural gas, this concept was later adopted for CO_2 capture [32,33]. The process schematic is depicted in Figure S-14. The main idea here is to harness the cooling power of accelerating supersonic flow to solidify and capture CO_2 from post-combustion exhaust gas [32–34].

The compressed exhaust gas is first accelerated through a converging/diverging nozzle to supersonic speed. As a result, the acceleration decreases the temperature of the exhaust gas, allowing condensable gas components, such as CO_2 , to be solidified. The deposited CO2 is then separated by inertial separation. The compression pressure depends on the flue gas concentration and the capture rate. The CO_2-lean gas undergoes deceleration in a diffuser to recover some pressure before atmospheric discharge [34].

The solid CO_2 particles are then pressurized using solid pumping, followed by heating to melt the CO_2 into a liquid and further liquid pumping and heating to transform CO_2 into a supercritical fluid. Since this occurs at significantly sub-ambient temperatures, thermal integration is essential to cool the exhaust gas, thereby facilitating the cryogenic capture.

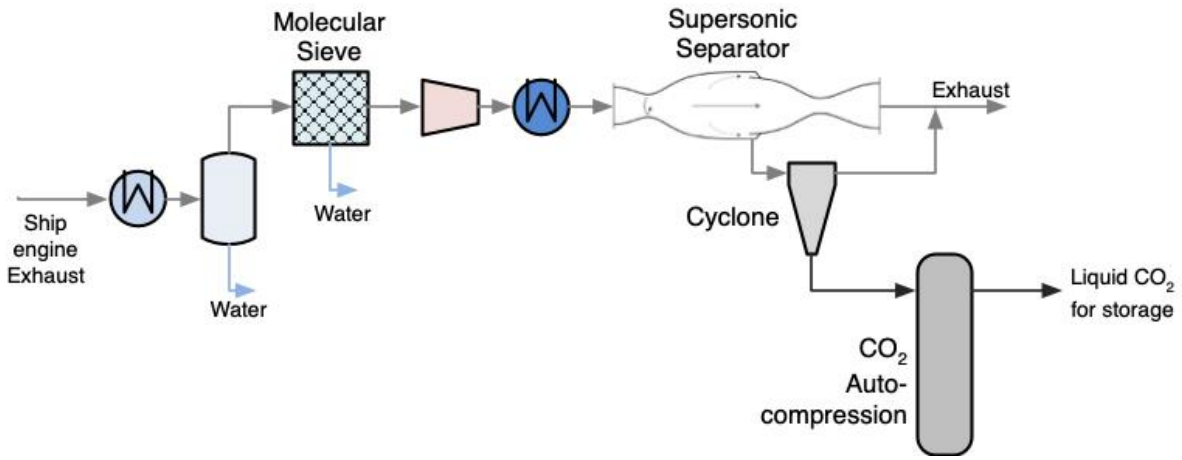

Figure S-14. Supersonic separation process scheme.

The converging/diverging nozzle is modeled using an in-house process model developed in C, which accurately reflects the CO_2 phase changes at supersonic conditions. This unit operation is then integrated into ASPEN HYSYS to perform overall steady-state process simulations [33]. The preliminary evaluation demonstrated that this technology could be a viable option for capturing CO_2 [33]. Although this technology has a low TRL, the small number of process units and the absence of gas-liquid or gas-solid interfaces make it attractive for marine vessels, which have limited space. Therefore, this concept is considered for the retrofit case to assess its potential, while it is excluded from the newbuilding scenario due to the need for high performance, given its low TRL.

S.3 Capture and conditioning process specifications

Table S-6. Specifications of the absorption CO_2 capture process.

Item	Unit	Value
DCC		
Packing material	-	MELLAPAK 250X
Packing height	m	5
Absorber		
Packing material	-	MELLAPAK 250X
Packing height	m	10
Lean solvent fraction	wt% MEA	30
Lean solvent loading	mol CO_2 / mol solvent	0.21
Water wash		
Packing material	-	MELLAPAK 250X
Packing height	m	1.5
Lean-rich heat exchanger		
Minimum temperature difference (ΔT_{min})	°C	10
Stripper		
Packing material	-	MELLAPAK 250X
Packing height	m	9
Stripper reboiler		
Heat source	-	Saturated steam
Heat exchanger ΔT_{min}	°C	10
Stripper condenser		
Heat sink	-	Cooling water
Heat exchanger ΔT_{min}	°C	10
Solvent degradation	wt%	0.02%

The simulation parameters used for both four-step and six-step VSA cycles are tabulated in Table S-7. The readers are referred to our previous study for CO_2 and N_2 dual-site Langmuir isotherm parameters [18].

Table S-7. Specifications of the VSA CO_2 capture process.

Item	Unit	Value
Column length-to-diameter ratio	-	2
Particle diameter	Mm	4
Bed porosity	-	0.37
Tortuosity	-	3
Particle porosity	-	
Particle density	kg/m^3	1130
Molecular diffusivity	cm^2/s	0.16
Fluid viscosity	cP	0.0172
Specific heat capacity of the adsorbent	J/kg/K	1070
Specific heat capacity of the gas phase	J/mol/K	30.1
Specific heat capacity of the adsorbed phase	J/mol/K	30.1
Effective thermal conductivity	W/m/K	0.09
Universal gas constant	J/mol/K	8.314
Exhaust gas pressure	Bar	1.013
Inlet feed temperature	K	298.15

Table S-8. Lower and upper bounds of key decision variables in VSA process optimizations.

Variable	Lower bound	Upper bound
Adsorption step duration (s)	50	500
Blowdown vacuum pump velocity (m/s)	0.4	2.5
Evacuation vacuum pump velocity (m/s)	0.4	2.5
Intermediate vacuum in the blowdown step (bar)	0.05	0.5
Low vacuum in the evacuation step (bar)	0.01	0.1
Column length (m)	6	9
Purge vacuum pump velocity (m/s)	0.2	1
Fractional reflux duration (-)	0.1	0.99

Table S-8. Specifications of the calcium-looping CO_2 capture process.

Item	Unit	Value
CaO density	kg/m^3	1660
$CaCO_3$ density	kg/m^3	2710
Carbonator operating temperature	°C	600
Carbonator operating pressure	Bara	1
CaO make-up ratio	%	5
Decay rate constant	-	0.39
Residual capacity	mol CO2/mol CaO	0.075
Number of cycles	-	25
Fraction of particles	-	0.05
Minimum temperature difference above ambient T		
Gas/gas	°C	20
Solid/Solid	°C	10

Table S-9. The specifications of rotating machinery in the onboard CCS facility.

Item	Unit	Value
Blower/Compressor		
Type	-	Centrifugal
Adiabatic efficiency	%	85
Maximum pressure ratio	-	4.0
Pump		
Type	-	Centrifugal
Adiabatic efficiency	%	80
Vacuum pump		
Type	-	Water-sealed
Adiabatic efficiency	%	75
Minimum inlet pressure	bara	0.2
Minimum outlet pressure	bara	1.03
Expander		
Type	-	Turbo
Adiabatic efficiency	%	85
Minimum outlet pressure	bara	1.1
Generator		
Efficiency	%	95

Table S-10. The specifications of heat exchangers in the onboard CCS facility.

Item	Unit	Value
Type		
Above ambient	-	Plate frame
Below ambient	-	Plate fin
Minimum temperature difference above ambient T		
Dusty gas/gas	°C	40
Dusty gas/liquid	°C	80
Liquid/liquid	°C	10
Condenser and intercooler	°C	10
Minimum temperature difference below ambient T		
General	°C	3
Boiling liquid/condensing liquid	°C	5
Heat exchanger pressure drops		
Liquid phase	bara	Max. 0.4
Gas phase	% of inlet	2.0
Water cooler		
Type	-	Plate frame
Outlet temperature	°C	46
Minimum temperature difference	°C	10

Table S-11. The ambient and cooling water conditions.

Item	Unit	Value
Air		
Temperature	°C	25
Pressure	bara	1.01
Relative humidity	%	60
Sea water		
Temperature	°C	32
Pressure	bara	1.01
Cooling water		
Cooling system	-	Indirect cooling
Cooling water supply T	°C	36
Cooling water supply p	bara	4.0
Cooling water return T	°C	46

Table S-12. CO_2 specifications from the Northern light project [35].

Item	Unit	Value
CO_2 capture rate	%	var
CO_2 storage condition	-	-
Phase	-	liquid
Temperature	°C	-
Pressure	barg	13-15
Purity	mol%	> 99.5
Impurities		
H_2O	ppm mol	<30
O_2	ppm mol	<10
SOx	ppm mol	<10
NOx	ppm mol	<10
H_2S	ppm mol	<9
CO	ppm mol	<100
Amine	ppm mol	<10
NH_3	ppm mol	<10
H_2	ppm mol	<50
Formaldehyde	ppm mol	<20
Acetaldehyde	ppm mol	<20
Mercury	ppm mol	<0.03
Cd and TI	ppm mol	<0.03

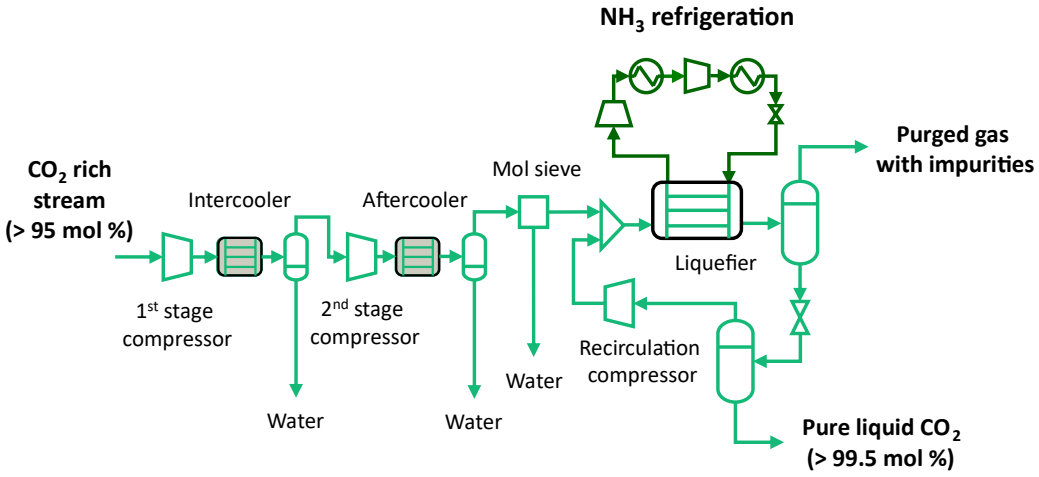

Figure S-15. Process flow diagram of CO_2 purification and liquefaction system [1].

Table S-13. Summary of available space for CO_2 capture and storage onboard [36].

Location	W [m]	L [m]	max. area [m^2]	max. height [m]	max. volume [m^3]
Funnel side B deck	-	-	40	12	480
Funnel side C deck	-	-	40	8	320
Funnel side D deck	-	-	40	6	240
A deck	10	10	100	18	1800
B deck extension	5	10	50	15	750
C deck extension	10	10	100	12	1200
Total for CO_2 capture*	-	-	220	-	2840
Between hatch 6-7	6	5	30	10	3110
On hatch 7 bottom left	8	8	64	10	3990
Total for CO_2 storage**	-	-	30	10	3110

*When “A deck” is selected for CO_2 capture.

**When “Between hatch 6-7” is selected for CO_2 storage to minimize cargo storage space loss.

S.4 Process simulation results

Table S-14. Simulation results of the retrofit (HFO) and newbuilding case (HFO-EGR).

Parameter	Unit	HFO No CCS	HFO-EGR No CCS	HFO MEA+liq	HFO-EGR MEA+liq	HFO-EGR MEA+liq
Flue gas to CCS	%	100	100	100	100	100
CO_2 capture rate	%	0	0	76.6	90	95
Final exhaust gas temperature	°C	259	258	254	251	250
Final exhaust gas CO_2 concentration	mol%	6.1	8.2	6.8	8.4	8.6
Specific heat demand - capture	$MJ/kgCO2_{captured}$	0	0	3.6	3.7	4.6
Specific power demand - capture	$MJ/kgCO2_{captured}$	0	0	0.6	0.4	0.4
Specific power demand - liquefaction	$MJ/kgCO2_{captured}$	0	0	0.4	0.4	0.4
Heat balance						
Heat baseload on ship	MW_{th}	2.2	2.2	2.2	2.2	2.2
Required heat for CCS	MW_{th}	0	0	5.9	8.2	11.9
Total heat demand on ship	MW_{th}	2.2	2.2	8.1	10.4	14.1
Economizer output	MW_{th}	1.4	1.0	1.8	1.6	2.3
CaL heat output	MW_{th}	0	0	0	0	0
Aux. boiler total duty	MW_{th}	0.8	1.2	6.3	8.8	11.7
Auxiliary boiler total load	%	13.5	18.5	100	139.8	186.2
Total heat production	MW_{th}	2.2	2.2	8.1	10.4	14.1
Power balance						
Required power for CCS	MW_{el}	0	0	1.6	1.9	2.1
Electricity baseload on ship	MW_{el}	0.5	0.5	0.5	0.5	0.5
Total electricity demand on ship	MW_{el}	0.5	0.5	2.1	2.4	2.6
ORC power generation	MW_{el}	0	0	0	0	0
Aux. engine total duty	MW_{el}	0.5	0.5	2.1	2.4	2.6
Aux. engine total load	%	15	15	63.4	70.8	78.7
Total power production	MW_{el}	0.5	0.5	2.1	2.4	2.6
Fuel usage						
Fuel for main engine baseload	kgfuel/h	1379	1379	1379	1379	1379
Fuel for aux. boiler baseload	kgfuel/h	86.1	118.0	86.1	118.0	118.0
Fuel for aux. engine baseload	kgfuel/h	90	90	90	90	90
Fuel for total baseload	kgfuel/h	1555	1587	1555	1587	1587
Extra fuel consumed for heat for CCS	kgfuel/h	0	0	551	773	1068
Extra fuel consumed for el. for CCS	kgfuel/h	0	0	289	334	38
Total extra fuel consumed for CCS	kgfuel/h	0	0	840	1107	1449
CO_2 emissions						
CO_2 emissions from main engine	kgCO2/h	4391	4457	4391	4457	4457
CO_2 emissions from aux. engines	kgCO2/h	302	302	1271	1421	1579
CO_2 emissions from aux. boiler	kgCO2/h	276	378	2042	2856	3803
Total CO_2 emissions	kgCO2/h	4969	5137	7705	8734	9840
Captured CO_2	kgCO2/h	0	0	5904	7861	9348
Net CO_2 emissions	kgCO2/h	4969	5137	1801	873	492
CO_2 emissions from ship without CCS	kgCO2/h	4969	5137	4969	5138	5138
CO_2 reduction rate	%	0	0	63.8	83	90.4
Extra fuel consumption rate	%	0	0	54.0	69.7	91.3
Extra fuel to avoided CO_2	$kgfuel_{extra}/kgCO2_{avoided}$	-	-	0.27	0.26	0.31
Specific CO_2 emissions	$gCO2/MJ_{fuel}$	78.9	79.9	18.6	8.0	4.0

Table S-14. Simulation results of the retrofit (HFO) and newbuilding case (HFO-EGR) (continued).

Parameter	Unit	HFO VSA-liq	HFO-EGR VSA-liq	HFO-EGR VSA-liq
Flue gas to CCS (or to MEA)	%	100	100	100
CO_2 capture rate	%	60.7	90	95
Temperature of engine exhaust	°C	260	260	260
Final exhaust gas CO_2 concentration	mol%	6.0	7.0	6.3
Specific heat demand - capture	$MJ/kgCO2_{captured}$	0	0	0
Specific power demand - capture	$MJ/kgCO2_{captured}$	2.2	2.4	4.6
Specific power demand - liquefaction	$MJ/kgCO2_{captured}$	0.4	0.5	0.5
Heat baseload on ship	MW_{th}	2.2	2.2	2.2
Required heat for CCS	MW_{th}	0	0	0
Total heat demand on ship	MW_{th}	2.2	2.2	2.2
Economizer output	MW_{th}	1.82	2.02	2.20
CaL heat output	MW_{th}	-	-	-
Aux. boiler total duty	MW_{th}	0.4	0.2	0
Auxiliary boiler total load	%	6.1	2.9	0
Total heat production	MW_{th}	2.2	2.2	2.2
Required power for CCS	MW_{el}	2.8	5.9	30.5
Electricity baseload on ship	MW_{el}	0.5	0.5	0.5
Total electricity demand on ship	MW_{el}	3.3	6.4	31.0
ORC power generation	MW_{el}	0	0	0.4
Aux. engine total duty	MW_{el}	3.3	6.4	30.6
Aux. engine total load	%	100	194	921
Total power production	MW_{el}	3.3	6.4	31
Fuel for main engine baseload	kgfuel/h	1379	1400	1400
Fuel for aux. boiler baseload	kgfuel/h	86.1	118	118
Fuel for aux. engine baseload	kgfuel/h	90	90	90
Fuel for total baseload	kgfuel/h	1555	1608	1608
Extra fuel consumed for heat for CCS	kgfuel/h	-47.4	-99.7	-118
Extra fuel consumed for el. for CCS	kgfuel/h	509	1069	5490
Total extra fuel consumed for CCS	kgfuel/h	461.	970	5372
CO_2 emissions from main engine	kgCO2/h	4391	4458	4458
CO_2 emissions from aux. engines	kgCO2/h	2006	3886	18466
CO_2 emissions from aux boiler	kgCO2/h	124	58.6	0
Total CO_2 emissions	kgCO2/h	6521	8402	22924
Captured CO_2	kgCO2/h	3957	7335	21124
Net CO_2 emissions	kgCO2/h	2564	1067	1800
CO_2 emissions from ship without CCS	kgCO2/h	4969	5138	5138
CO_2 reduction rate	%	48.4	79.2	65.0
Extra fuel consumption rate	%	29.6	65.7	349
Extra fuel to avoided CO_2	$kgfuel_{extra}/kgCO2_{avoided}$	0.19	0.24	1.61
Specific CO_2 emissions	$gCO2/MJ_{fuel}$	91.4	27.6	16.4

Table S-14. Simulation results of the retrofit (HFO) and newbuilding case (HFO-EGR) (continued).

Parameter	Unit	HFO Mem-liq	HFO-EGR Mem-liq	HFO-EGR Mem-liq	HFO Cryo
Flue gas to CCS	%	100	100	100	100
CO_2 capture rate	%	58.8	90	95	60
Temperature of engine exhaust	°C	260	260	260	260
Final exhaust gas CO_2 concentration	mol%	6.0	7.0	6.8	6.0
Specific heat demand - capture	$MJ/kgCO2_{captured}$	0	0	0	0
Specific power demand - capture	$MJ/kgCO2_{captured}$	2.7	2.7	3.2	2.6
Specific power demand - liquefaction	$MJ/kgCO2_{captured}$	0	0	0	0
Heat balance					
Heat baseload on ship	MW_{th}	2.2	2.2	2.2	2.2
Required heat for CCS	MW_{th}	0	0	0	0
Total heat demand on ship	MW_{th}	2.2	2.2	2.2	2.2
Economizer output	MW_{th}	1.8	1.9	2.2	1.8
CaL heat output	MW_{th}	0	0	0	0
Aux. boiler total duty	MW_{th}	0.4	0.3	0	0.4
Auxiliary boiler total load	%	6.1	4.3	0	6.1
Total heat production	MW_{th}	2.2	2.2	2.2	2.2
Power balance					
Required power for CCS	MW_{el}	2.8	5.4	8.1	2.8
Electricity baseload on ship	MW_{el}	0.5	0.5	0.5	0.5
Total electricity demand on ship	MW_{el}	3.3	5.9	8.6	3.3
ORC power generation	MW_{el}	0.0	0	0	0
Aux. engine total duty	MW_{el}	3.3	5.9	8.5	3.3
Aux. engine total load	%	100	178	257	100
Total power production	MW_{el}	3.3	5.9	8.6	3.3
Fuel usage					
Fuel for main engine baseload	kgfuel/h	1379	1379	1379	1379
Fuel for aux. boiler baseload	kgfuel/h	86.1	118.0	118.0	86.1
Fuel for aux. engine baseload	kgfuel/h	90	90	90	90
Fuel for total baseload	kgfuel/h	1555	1587	1587	1555
Extra fuel consumed for heat for CCS	kgfuel/h	-47.4	-91.5	-118	-47.4
Extra fuel consumed for el. for CCS	kgfuel/h	509	974	1452	509
Total extra fuel consumed for CCS	kgfuel/h	461	883	1334	461
CO_2 emissions					
CO_2 emissions from main engine	kgCO2/h	4391	4458	4458	4391
CO_2 emissions from aux. engines	kgCO2/h	2006	3568	5158	2006
CO_2 emissions from aux boiler	kgCO2/h	124	85	0	124
Total CO_2 emissions	kgCO2/h	6521	8111	9616	6521
Captured CO_2	kgCO2/h	3838	7300	9135	3912
Net CO_2 emissions	kgCO2/h	2684	811	481	2610
CO_2 emissions from ship without CCS	kgCO2/h	4969	5138	5138	4970
CO_2 reduction rate	%	46	84.2	90.6	47.5
Extra fuel consumption rate	%	29.6	55.6	84.1	29.6
Extra fuel to avoided CO_2	$kgfuel_{extra}/kgCO2_{avoided}$	0.2	0.2	0.29	0.2
Specific CO_2 emissions	$gCO2/MJ_{fuel}$	32.9	8.1	4.1	32

Table S-14. Simulation results of the retrofit (HFO) and newbuilding case (HFO-EGR) (continued).

Parameter	Unit	HFO CaL	HFO-EGR CaL	HFO-EGR CaL	HFO-EGR CaL+MEA
Flue gas to CCS*	%	68.46	93.12	99.12	55.75
CO_2 capture rate	%	90	90	90	90
Temperature of engine exhaust	°C	260	260	260	260
Final exhaust gas CO_2 concentration	mol%	6.0	8.0	8.0	7.9
Specific heat demand - capture	$MJ/kgCO2_{captured}$	0	0	0	3.8
Specific power demand - capture	$MJ/kgCO2_{captured}$	0	0	0	0.3
Specific power demand - liquefaction	$MJ/kgCO2_{captured}$	0	0	0	0.4
Heat balance					
Heat baseload on ship	MW_{th}	2.2	2.2	2.2	2.2
Required heat for CCS	MW_{th}	0	0	0	2.1
Total heat demand on ship	MW_{th}	2.2	2.2	2.2	4.3
Economizer output	MW_{th}	0	0	0	0.5
CaL heat output	MW_{th}	4.8	6.0	6.4	3.8
Aux. boiler total duty	MW_{th}	0	0	0	0
Auxiliary boiler total load	%	0	0	0	0
Total heat production	MW_{th}	4.8	6.0	6.4	4.3
Power balance					
Required power for CCS	MW_{el}	0	0	0	0.4
Electricity baseload on ship	MW_{el}	0.5	0.5	0.5	0.5
Total electricity demand on ship	MW_{el}	0.5	0.5	0.5	0.9
ORC power generation	MW_{el}	0	0	0	00
Aux. engine total duty	MW_{el}	0.5	0.5	0.5	0.9
Aux. engine total load	%	15	15	15	27
Total power production	MW_{el}	0.5	0.5	0.5	0.9
Fuel usage					
Fuel for main engine baseload	kgfuel/h	1379	1379	1379	1379
Fuel for aux. boiler baseload	kgfuel/h	86.1	118	118	118
Fuel for aux. engine baseload	kgfuel/h	90	90	90	90
Fuel for total baseload	kgfuel/h	1555	1587	1587	1587
Extra fuel consumed for heat for CCS	kgfuel/h	-86.1	-118.0	-118	-118
Extra fuel consumed for el. for CCS	kgfuel/h	0	0	0	71.8
Total extra fuel consumed for CCS	kgfuel/h	-86.1	-118	-118	-46.2
CO_2 emissions					
CO_2 emissions from main engine	kgCO2/h	439	4458	4458	4458
CO_2 emissions from aux. engines	kgCO2/h	302	302	302	542
CO_2 emissions from aux boiler	kgCO2/h	0	0	0	0
Total CO_2 emissions	kgCO2/h	4693	4759	4759	5000
Captured CO_2	kgCO2/h	2892	3989	4245	1991
Net CO_2 emissions	kgCO2/h	1801	771	514	500
CO_2 emissions from ship without CCS	kgCO2/h	4969	5137.6	5138	5138
CO_2 reduction rate	%	63.8	85.0	90	90.3
Extra fuel consumption rate	%	-5.5	-7.4	-7.4	-2.9
Extra fuel to avoided CO_2	$kgfuel_{extra}/kgCO2_{avoided}$	-0.03	-0.03	-0.03	-0.01
Specific CO_2 emissions	$gCO2/MJ_{fuel}$	30.3	13.0	8.6	8.0

*Flue gas to the CaL capture system in the CaL and CaL+MEA system.

Table S-15. Validation of the process performance based on the optimal solutions predicted by VSA neural network (ANN) models against the rigorous VSA process models (RPM) for retrofit and newbuilding cases.

Parameter	Retrofit		Newbuilding (90%)		Newbuilding (95%)	
	ANN	RPM	ANN	RPM	ANN	RPM
Adsorption feed pressure (bar)	1.05	1.05	1.05	1.05	1.05	1.05
Intermediate vacuum (bar)	0.15	0.15	0.10	0.1	0.07	0.07
Low vacuum (bar)	0.031	0.031	0.017	0.017	0.010	0.010
BLO vacuum pump velocity (m/s)	0.84	0.84	1.04	1.04	1.19	1.19
EVAC vacuum pump velocity (m/s)	0.41	0.41	1.64	1.64	0.99	0.99
Adsorption step duration (s)	219	219	91	91	113	113
Column length (m)	7.4	7.4	6.7	6.7	6.6	6.6
Purge vacuum pump velocity (m/s)	-	-	0.65	0.65	0.94	0.94
Fractional reflux duration (-)	-	-	0.99	0.99	0.91	0.91
Blowdown time (s)	172	167	170	186	158	198
Evacuation time (s)	1546	1697	414	467	1160	1203
VSA purity (%)	81.6	82.2	76.7	72.3	81.8	78.5
VSA recovery (%)	57.7	56.5	95.3	95.1	96.9	96.2
VSA power consumption (kW)	2284	22316	6229	6883	7561	7192

S.5 Footprint of capture processes

Table S-16. Footprint of main equipment in the absorption system for the retrofit (HFO) and newbuilding case (HFO-EGR).

Equipment		Diameter	Area	Height	Volume
		m	m^2	m	m^3
HFO MEA+liq	DCC	3.0	7	8	56
	Absorber and Waterwash	4.2	14	16	224
	Desorber	2.3	4	15	60
	Liquefier	-	41	2	82
HFO-EGR MEA+liq 90%CCR	DCC	3.0	7	8	56
	Absorber and Waterwash	4.5	16	16	256
	Desorber	2.8	6	15	90
	Liquefier	-	45	2	90
HFO-EGR MEA+liq 95% CCR	DCC	3.2	8	8	64
	Absorber and Waterwash	4.8	18	16	288
	Desorber	3.2	8	15	120
	Liquefier	-	50	2	100
HFO-EGR CaL/MEA+liq 90%CCR	DCC	1.8	3	8	20
	Absorber and Waterwash	2.8	6	16	96
	Desorber	1.4	2	15	24
	Liquefier	-	18	2	36

Table S-17. Footprint of main equipment in the adsorption-liquefaction hybrid system for the retrofit (HFO) and newbuilding case (HFO-EGR).

Item	Unit	HFO	HFO-EGR 90%CCR	HFO-EGR 95%CCR
Column diameter	m	3.7	3.3	3.3
Column height	m	6	6	6
Number of columns per train	-	9	9	15
Number of trains	-	1	2	2
Total column area	m^2	96	157	259
Total column volume	m^3	576	942	1554
Liquefier	m^3	40	75	60
Total	m^3	616	1017	1614

Table S-18. Footprint of main equipment in the membrane-assisted liquefaction system for the retrofit (HFO) and newbuilding case (HFO-EGR) [37].

Case	Membrane module volume	Membrane module capacity	Membrane area	Number of modules	Membrane module volume	Liquefier volume
	m^3/module	m^2/module	m^2	[-]	m^3	m^3
HFO	0.03	20	19221	961	31	77
HFO-EGR: 90 %CCR	0.03	20	52489	2624	85	90
HFO-EGR: 95 %CCR	0.03	20	75799	3790	123	140

Table S-19. Footprint of main equipment in the cryogenic supersonic process for the retrofit (HFO) case.

Item	Unit	HFO
Nozzle length	m	4.0
Nozzle width	m	4
Nozzle height	m	4
Nozzle volume	m^3	64

Table S-20. Footprint of main equipment in the CaL and CaL-MEA hybrid system for the retrofit (HFO) and newbuilding case (HFO-EGR).

Item	Unit	CaL HFO	CaL HFO-EGR 90% CCR eqv.	CaL HFO-EGR 95% CCR eqv.	CaL-MEA+Liq HFO-EGR 95% CCR eqv.
Carbonator diameter	m	6.5	6.6	6.8	5.2
Carbonator height	m	10	10	10	10
Carbonator volume	m^3	331	338	360	216

Reference

[1] Deng H, Roussanaly S, Skaugen G. Techno-economic analyses of CO2 liquefaction: Impact of product pressure and impurities. International Journal of Refrigeration 2019;103:301–15. https://doi.org/10.1016/j.ijrefrig.2019.04.011.

[2] Rezazadeh F, Gale WF, Rochelle GT, Sachde D. Effectiveness of absorber intercooling for CO2 absorption from natural gas fired flue gases using monoethanolamine solvent. International Journal of Greenhouse Gas Control 2017;58:246–55. https://doi.org/10.1016/j.ijggc.2017.01.016.

[3] Gao T, Rochelle GT. Creative absorber design and optimization for CO2 capture with aqueous piperazine. International Journal of Greenhouse Gas Control 2022;113:103534. https://doi.org/10.1016/j.ijggc.2021.103534.

[4] Suresh Babu A, Rochelle GT. Process design of the piperazine advanced stripper for a 460 MW NGCC. International Journal of Greenhouse Gas Control 2022;115:103631. https://doi.org/10.1016/j.ijggc.2022.103631.

[5] Oh J, Kim D, Roussanaly S, Anantharaman R, Lim Y. Optimal capacity design of amine-based onboard CO2 capture systems under variable marine engine loads. Chemical Engineering Journal 2024;483:149136. https://doi.org/10.1016/j.cej.2024.149136.

[6] IEAGHG. Understanding the Cost of Retrofitting CO2 capture in an Integrated Oil Refinery. 2017.

[7] Gardarsdottir SO, De Lena E, Romano M, Roussanaly S, Voldsund M, Pérez-Calvo J-F, et al. Comparison of Technologies for CO2 Capture from Cement Production—Part 2: Cost Analysis. Energies 2019;12:542. https://doi.org/10.3390/en12030542.

[8] Anantharaman R, Berstad D, Roussanaly S. Techno-economic Performance of a Hybrid Membrane – Liquefaction Process for Post-combustion CO2 Capture. Energy Procedia 2014;61:1244–7. https://doi.org/10.1016/j.egypro.2014.11.1068.

[9] Zhang X, He X, Gundersen T. Post-combustion Carbon Capture with a Gas Separation Membrane: Parametric Study, Capture Cost, and Exergy Analysis. Energy & Fuels 2013;27:4137–49. https://doi.org/10.1021/ef3021798.

[10] Bouma R, Vercauteren F, van Os P, Goetheer E, Berstad D, Anantharaman R. Membrane-assisted CO2 Liquefaction: Performance Modelling of CO2 Capture from Flue Gas in Cement Production. Energy Procedia 2017;114:72–80. https://doi.org/10.1016/j.egypro.2017.03.1149.

[11] Lindqvist K, Roussanaly S, Anantharaman R. Multi-stage Membrane Processes for CO2 Capture from Cement Industry. Energy Procedia 2014;63:6476–83. https://doi.org/10.1016/j.egypro.2014.11.683.

[12] Roussanaly S, Anantharaman R, Lindqvist K, Hagen B. A new approach to the identification of high-potential materials for cost-efficient membrane-based post-combustion CO2 capture. Sustainable Energy & Fuels 2018;2:1225–43. https://doi.org/10.1039/C8SE00039E.

[13] Subraveti SG, Roussanaly S, Anantharaman R, Riboldi L, Rajendran A. Techno-economic assessment of optimised vacuum swing adsorption for post-combustion CO2 capture from steam-methane reformer flue gas. Separation and Purification Technology 2021;256:117832. https://doi.org/10.1016/j.seppur.2020.117832.

[14] Haghpanah R, Nilam R, Rajendran A, Farooq S, Karimi IA. Cycle synthesis and optimization of a VSA process for postcombustion CO2 capture. AIChE Journal 2013;59:4735–48. https://doi.org/10.1002/aic.14192.

[15] Khurana M, Farooq S. Integrated Adsorbent Process Optimization for Minimum Cost of Electricity Including Carbon Capture by a VSA Process. AIChE Journal 2019;65:184–95. https://doi.org/10.1002/aic.16362.

[16] Estupiñan Perez L, Sarkar P, Rajendran A. Experimental validation of multi-objective optimization techniques for design of vacuum swing adsorption processes. Separation and Purification Technology 2019;224:553–63. https://doi.org/10.1016/j.seppur.2019.05.039.

[17] Krishnamurthy S, Rao VR, Guntuka S, Sharratt P, Haghpanah R, Rajendran A, et al. CO2 capture from dry flue gas by vacuum swing adsorption: A pilot plant study. AIChE Journal 2014;60:1830–42. https://doi.org/10.1002/aic.14435.

[18] Subraveti SG, Roussanaly S, Anantharaman R, Riboldi L, Rajendran A. How much can novel solid sorbents reduce the cost of post-combustion CO2<math><msub is="true"><mrow is="true"><mi mathvariant="normal" is="true">CO</mi></mrow><mrow is="true"><mn is="true">2</mn></mrow></msub></math> capture? A techno-economic investigation on the cost limits of pressure–vacuum swing adsorption. Applied Energy 2022;306:117955. https://doi.org/10.1016/j.apenergy.2021.117955.
[19] Pai KN, Prasad V, Rajendran A. Generalized, Adsorbent-Agnostic, Artificial Neural Network Framework for Rapid Simulation, Optimization, and Adsorbent Screening of Adsorption Processes. Ind Eng Chem Res 2020;59:16730–40. https://doi.org/10.1021/acs.iecr.0c02339.
[20] Burns TD, Pai KN, Subraveti SG, Collins SP, Krykunov M, Rajendran A, et al. Prediction of MOF Performance in Vacuum Swing Adsorption Systems for Postcombustion CO2 Capture Based on Integrated Molecular Simulations, Process Optimizations, and Machine Learning Models. Environ Sci Technol 2020;54:4536–44. https://doi.org/10.1021/acs.est.9b07407.
[21] Leperi KT, Yancy-Caballero D, Snurr RQ, You F. 110th Anniversary: Surrogate Models Based on Artificial Neural Networks To Simulate and Optimize Pressure Swing Adsorption Cycles for CO2 Capture. Ind Eng Chem Res 2019;58:18241–52. https://doi.org/10.1021/acs.iecr.9b02383.
[22] Sachio S, Ward A, Pini R, Papathanasiou MM. Operability-economics trade-offs in adsorption-based CO2 capture processes. Commun Eng 2024;3:1–10. https://doi.org/10.1038/s44172-024-00244-x.
[23] Subraveti SG, Anantharaman R. Methane enrichment from dilute sources: Performance limits and implications for methane removal and abatement 2025. https://doi.org/10.26434/chemrxiv-2025-q70cw-v2.
[24] Haghpanah R, Majumder A, Nilam R, Rajendran A, Farooq S, Karimi IA, et al. Multiobjective Optimization of a Four-Step Adsorption Process for Postcombustion CO2 Capture Via Finite Volume Simulation. Ind Eng Chem Res 2013;52:4249–65. https://doi.org/10.1021/ie302658y.
[25] Subraveti SG, Li Z, Prasad V, Rajendran A. Machine Learning-Based Multiobjective Optimization of Pressure Swing Adsorption. Ind Eng Chem Res 2019;58:20412–22. https://doi.org/10.1021/acs.iecr.9b04173.
[26] Optimization of pressure-vacuum swing adsorption processes for nitrogen rejection from natural gas streams using a nitrogen selective metal organic framework - Wilkins - 2022 - The Canadian Journal of Chemical Engineering - Wiley Online Library n.d. https://onlinelibrary.wiley.com/doi/full/10.1002/cjce.24469 (accessed May 19, 2025).
[27] Subraveti SG, Riboldi L, Xu HY, Jooss Y, Roussanaly S, Andersson LE, et al. How to accurately fast-track sorbent selection for post-combustion CO2 capture? A comparative assessment of data-driven and simplified physical models for screening sorbents. In: Kokossis AC, Georgiadis MC, Pistikopoulos E, editors. Computer Aided Chemical Engineering, vol. 52, Elsevier; 2023, p. 3013–8. https://doi.org/10.1016/B978-0-443-15274-0.50480-7.
[28] Arias B, Alonso M, Abanades C. CO2 Capture by Calcium Looping at Relevant Conditions for Cement Plants: Experimental Testing in a 30 kWth Pilot Plant. Ind Eng Chem Res 2017;56:2634–40. https://doi.org/10.1021/acs.iecr.6b04617.
[29] Sweeney B. RECAST - A system to decarbonise long-distance shipping. 2020.
[30] Kierzkowska AM, Pacciani R, Müller CR. CaO-Based CO2 Sorbents: From Fundamentals to the Development of New, Highly Effective Materials. ChemSusChem 2013;6:1130–48. https://doi.org/10.1002/cssc.201300178.
[31] Balepin V, Castrogiovanni A, Girlea F, Robertson A, Sforza P. Inertial extraction system. US20130228076A1, 2012.
[32] Forsyth J, Lodge S, Consonni S, Di Bona D, Gatti M, Martelli E, et al. Evaluation of Five Alternative CO2 Capture Technologies with Insights to Inform Further Development. Energy Procedia 2017;114:2599–610. https://doi.org/10.1016/j.egypro.2017.03.1419.
[33] Hammer M, Wahl PE, Anantharaman R, Berstad D, Lervåg KY. CO2 Capture from Off-shore Gas Turbines Using Supersonic Gas Separation. Energy Procedia 2014;63:243–52. https://doi.org/10.1016/j.egypro.2014.11.026.

[34] Berger AH, Wang Y, Bhown AS, Castrogiovanni A, Kielb R, Balepin V. Thermodynamic Analysis of Post-combustion Inertial CO2 Extraction System. Energy Procedia 2017;114:7–16. https://doi.org/10.1016/j.egypro.2017.03.1140.
[35] Equinor. Northern Lights FEED Report: RE-PM673-00057. Https://Northernlightsccs.Com/En/Facts-and-Reports: 2020.
[36] Tavakoli S, Gamlem GM, Kim D, Roussanaly S, Anantharaman R, Yum KK, et al. Exploring the technical feasibility of carbon capture onboard ships. Journal of Cleaner Production 2024;452:142032. https://doi.org/10.1016/j.jclepro.2024.142032.
[37] Kniep, Jay, Sun Z, Lin H, Mohammad M, He Z, Merkel T, et al. FIELD TESTS OF MTR MEMBRANES FOR SYNGAS SEPARATIONS: Final Report of CO2-Selective Membrane Field Test Activities at the National Carbon Capture Center. Membrane Technology and Research, Inc.; 2017.